Accepted Manuscript

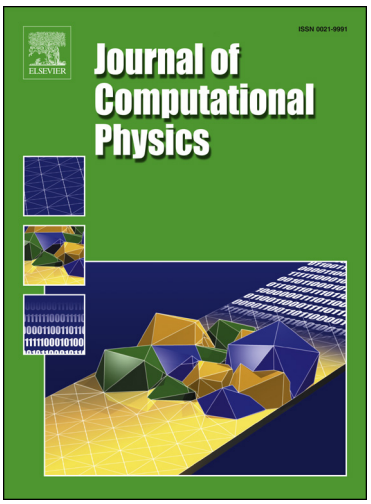

Nano–particle drag prediction at low Reynolds number using a direct Boltzmann–BGK solution approach

B. Evans

PII: S0021-9991(17)30698-8
DOI: https://doi.org/10.1016/j.jcp.2017.09.038
Reference: YJCPH 7611

To appear in: *Journal of Computational Physics*

Received date: 15 March 2017
Revised date: 26 July 2017
Accepted date: 21 September 2017

Please cite this article in press as: B. Evans, Nano–particle drag prediction at low Reynolds number using a direct Boltzmann–BGK solution approach, *J. Comput. Phys.* (2017), https://doi.org/10.1016/j.jcp.2017.09.038

Highlights

- A novel finite element approach for solution of the Boltzmann-BGK equation.
- Nano-particle drag prediction.
- Drag predictions are aligned well with alternative numerical approaches.
- Significance of molecular wall absorption assumptions demonstrated.
- Applications in a range of fields, including medical, is outlined.

Nano–particle drag prediction at low Reynolds number using a direct Boltzmann–BGK solution approach

B. Evans[1,*]

Abstract

This paper outlines a novel approach for solution of the Boltzmann-BGK equation describing molecular gas dynamics applied to the challenging problem of drag prediction of a 2D circular nano–particle at transitional Knudsen number (0.0214) and low Reynolds number (0.25 - 2.0). The numerical scheme utilises a discontinuous-Galerkin finite element discretisation for the physical space representing the problem particle geometry and a high order discretisation for molecular velocity space describing the molecular distribution function. The paper shows that this method produces drag predictions that are aligned well with the range of drag predictions for this problem generated from the alternative numerical approaches of molecular dynamics codes and a modified continuum scheme. It also demonstrates the sensitivity of flow-field solutions and therefore drag predictions to the wall absorption parameter used to construct the solid wall boundary condition used in the solver algorithm. The results from this work has applications in fields ranging from diagnostics and therapeutics in medicine to the fields of semiconductors and xerographics.

Keywords: nano–particle, drag, Boltzmann, molecular dynamics, discontinuous Galerkin, finite element

1. Introduction

1.1. Background to the Problem

As the scale of possible practical engineering structures continues to reduce to the nano–scale, the demand to be able to predict the behaviour of such structures of this size within fluid flows is becoming increasingly significant. The principles of molecular biomechanics have, in recent years, allowed the development of microscale devices that are sub 100nm in length–scale [1]. To put this into context, a red blood cell has a diameter of the order 6,000–8,000nm[2], a rod–shaped E-coli bacterium has a length of 2,500nm [3], a human DNA molecule has a typical length scale of the order 2-3nm[4] and an individual atom is typically a fraction of a nano–metre.

Nano–scale devices (or nano–particles) can be made of a range of materials including lipids, metals and natural or synthetic polymers[5] at length scales ranging from 1 to 100nm. They have been employed in medical applications for both therapeutic and diagnostic purposes over the past two decades [5]. It has, more recently, been acknowledged [6] that an improved understanding of the mechanical forces (drag) acting on particles at this scale will result in significant improvements in, for example, the efficacy of targeting of cancer molecules in therapies involving the use of nano–particles for cancer treatment delivery [7]. Nano–particles used for this type of drug delivery are now being trialled at scales of sub 10nm [8]. In the work of Kingsley et al [9] and

*Corresponding Author: Tel.: +441792602129
Email address: b.j.evans@swansea.ac.uk (B. Evans)

Uhrich et al [10] it has been noted that despite the use of nano–scale therapeutic devices in medicine for many years, targeting capabilities are still poor and that this is largely due to inabilities to predict drag forces on nano–devices accurately.

Other applications involving nano–particles that would benefit from improved flowfield simulation capabilities include applications in the semiconductor, pharmarceutical and xerographic fields [11]. For example, the drag force on nano–particles has been used [12] to 'clean' structured nano–scale surfaces.

The forces acting on a particle at the molecular scale can be sub-divided into three types: mechanical, thermal and chemical. This paper explores a modelling method that considers the first two (mechanical and thermal) of these force types. The mechanical (viscous) force is of fundamental importance in diffusion processes whereas the thermal (collisional) force is defined as that which takes place when molecules collide with each other. Thermal forces tend to drive movement within a molecular flowfield and (as will be shown) are the dominant source of drag on a nano–particle.

A review of the literature quickly leads to the conclusion that modelling the drag on particles below 100nm in dimension remains a highly challenging topic of study. This is exacerbated by the fact that at this scale there are no direct analytical solutions or experimental data available with which to compare simulation results. The majority of work in this field has been undertaken by practioners using either a boundary condition adapted continuum approach [13] or a molecular dynamics approach [5] and different schemes produce relatively large differences in predicted drag coefficients as a function of Reynolds number in the transitional region of the Knudsen regime. For this reason, this paper focusses on the solution of a relatively simple problem i.e. predicting the relationship between the drag coefficient, C_d and Reynold's number, Re between $Re = 0.25$ and $Re = 2.0$ at a Knudsen number, Kn of 0.0214 on a 2nm diameter 2D circular particle in a channel of width 8nm (shown in Figure 1) since there is a range of simulation data available [5, 13, 14] against which the direct Boltzmann solution results can be compared.

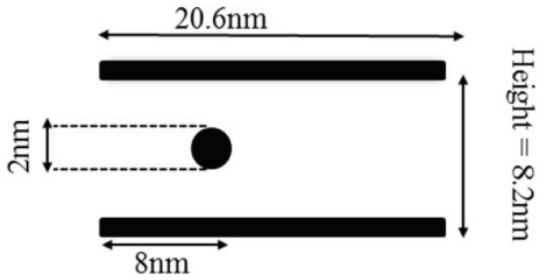

Figure 1: Particle geometry considered in this paper (adapted from [5])

In the remainder of this section of the paper the macroscopic and molecular approaches for studying fluids will be compared and contrasted in the context of the Knudsen regime before the Boltzmann and Boltzmann–BGK equations are introduced. This is followed by a literature review detailing approaches for solving the Boltzmann equation and phenomenological molecular modelling schemes that claim to produce solutions to the Boltzmann equation. In Section 2 the novel discontinuous–Galerkin finite element scheme for Boltzmann–BGK equation solution is outlined including a discussion on the implementation of the necessary boundary conditions at which point the important 'wall absorption parameter' is introduced. Section 3 sets out the results from the

set of simulations conducted as part of this work including flow–field predictions and drag coefficient predictions. These results are discussed and compared with results from molecular dynamics codes and a modified continuum (Navier–Stokes) approach. Finally in Section 4 the conclusions from this study are summarised and future work and potential improvements to the solver are outlined.

1.2. Fluids modelling approaches

A gas flow may be modelled at either the macroscopic or microscopic level. At the macroscopic level we must make the assumption that the gas properties can be regarded as continuous variables. If this assumption is reasonable then the Navier–Stokes equations provide the appropriate mathematical description of the physics of the flow.

We can classify a gas flow in terms of a non–dimensional parameter called the Knudsen number (Kn), defined as

$$Kn = \frac{\lambda}{L} \tag{1}$$

where λ is the mean free path of molecules in the flow, i.e. the average distance travelled between collisions, and L is some typical length scale in the flow. The traditional 'rule of thumb' for continuum assumption validity is that Kn should be less than 0.1 [30]. This can be misleading if L is chosen to be some overall dimension of the flow in order to define a single global Kn for the flow. The limit can be defined more precisely if we define a local Kn with L

$$L = \frac{\rho}{d\rho/dx} \tag{2}$$

as the scale length of the macroscopic gradients where ρ is the fluid density. The Knudsen number limits on the conventional formulations to describe gas flows is shown schematically in Figure 2

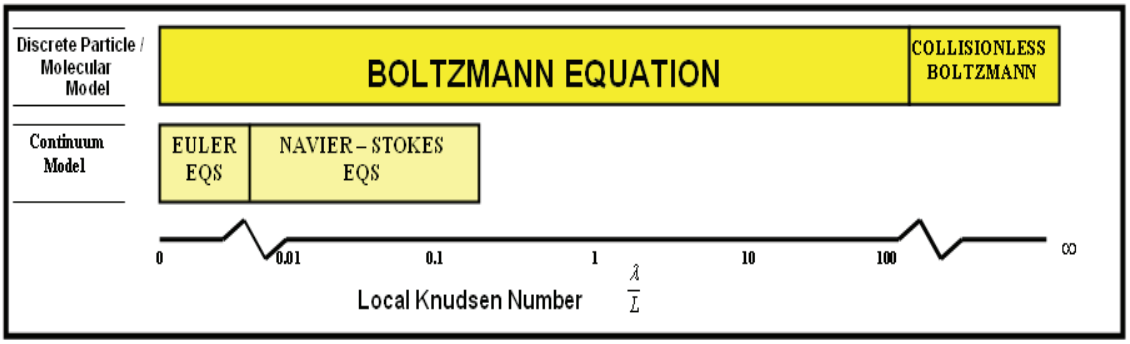

Figure 2: The Knudsen Regime [18]

This paper focusses on flows in the low Reynolds, Re region ($Re = 0.2 - 2.0$) at a global Knudsen number (based on particle diameter) of 0.0214. This places the problem in the 'transitional' region in the Knudsen regime where the validity of the traditional Navier–Stokes approach is beginning to break down, particularly with regards to the 'no slip' wall boundary condition. It is for this reason that a direct Boltzmann equation

solution approach (which in principle is valid across the full range of Kn) has been chosen and compared with both molecular dynamics solutions to this problem and boundary condition modified Navier–Stokes solutions.

1.3. Background to the Boltzmann–BGK Equation and solution approaches

1.3.1. The BGK simplification to the Boltzmann Equation

It will be useful at this stage to introduce the Boltzmann equation and its 'BGK form' simplification. Note that its derivation can be found in the following references [30, 62, 61]. The full Boltzmann equation can be written as,

$$\frac{\partial(nf)}{\partial t} + \boldsymbol{c}.\frac{\partial(nf)}{\partial \boldsymbol{r}} + \boldsymbol{F}.\frac{\partial(nf)}{\partial \boldsymbol{c}} = \frac{1}{Kn}Q(f,f) \tag{3}$$

where $f = f(\boldsymbol{r}, \boldsymbol{c}, t)$ is the distribution function, n is the molecular number density, $\boldsymbol{F}$ describes any force fields (gravitational, electrostatic etc) that might be present and $Q(f, f)$ is the term accounting for molecular collisions. Note that $\boldsymbol{c}$ here refers to the molecular velocity.

The Boltzmann equation is an integro–differential equation and analytical solutions are restricted to extremely simple applications [59, 60]. The term $Q(f, f)$ is a five-fold integral, in three spatial dimensions, and is the source of many of the difficulties in solving this equation. As a result of this, simplification of the Boltzmann equation is usually focussed on some form of complexity reduction of the collision term. The most useful of these simplifications by Bhatnagar, Gross and Krook [62] relies on the assumption that departures from thermodynamic equilibrium are relatively small and that the effect of collisions is to return a non–equilibrium molecular velocity distribution to equilibrium at a rate proportional to the molecular collision frequency such that the Boltzmann-BGK equation becomes,

$$\frac{\partial}{\partial t}(nf) + \boldsymbol{c}.\frac{\partial(nf)}{\partial \boldsymbol{r}} + \boldsymbol{F}.\frac{\partial(nf)}{\partial \boldsymbol{c}} = \nu(\boldsymbol{r}, t)((nf_0) - (nf)). \tag{4}$$

where $\nu(\boldsymbol{r}, t)$ is a term proportional to the molecular collision frequency and f_0 is the local Maxwellian equilibrium distribution function defined as,

$$f_0(\boldsymbol{c}) = (\frac{\beta^3}{\pi^{3/2}})\exp(-\beta^2(\boldsymbol{c} - \boldsymbol{c_0})^2) \tag{5}$$

in 3 dimensions where $\boldsymbol{c_0}$ is the bulk velocity of the flow and $\beta = (2RT)^{-1/2} = \sqrt{m/(2kT)}$. R is the gas constant, T is the gas temperature measured in Kelvin, m is the molecular mass and k is the Boltzmann constant (1.380 650524 x10^{-23} Joules/Kelvin). A helpful derivation of the Maxwellian distribution function is provided by Vincenti and Kruger in [61]. The inclusion of the equilibrium distribution function in the BGK term means that the Boltzmann-BGK equation is still a non–linear, integro–differential equation because f_0 is a function of the stream velocity, $\boldsymbol{c_0}$ and the temperature, T, which are obtained by taking integrals over f. However, computationally, the BGK term is significantly less demanding than the full Boltzmann equation right-hand side term. Solution of the Boltzmann–BGK equation will form the basis of all of the work presented in this paper.

1.3.2. Direct solution approaches for the Boltzmann equation

A class of methods that has the Boltzmann equation at its heart, although cannot be truly regarded as providing solutions of the Boltzmann equation, are lattice Boltzmann methods (LBMs), [19]. The LBM is a mesoscopic particle–based approach to simulate fluid flows and has become a serious alternative to traditional

methods in CFD for certain applications. The LBM is often derived from the simplified Boltzmann–BGK equation (see section 1.3.1). In lattice gases, particles 'live' on the nodes of a discrete lattice. Particles 'jump' from one node of the lattice to another according to their discrete velocities. This highly simplified view of the propagation of molecules differentiates it from the true Boltzmann solver detailed in this work in which no restrictions are placed on possible molecular velocities. In the LBM approach, particles may collide and acquire new discrete velocities in the 'collision phase'. This method is applied to three dimensional flows in pipes and around a sphere at moderate Reynolds numbers by Rossi et al [20] and an example of the treatment of boundaries is provided by Yu, Mei and Shyy [21]. There are many cases of the LBM being applied to microchannel flows, thermal problems and mesoscale flows in the literature [22, 23, 24]. However, the author is unaware of any successful attempts to use the LBM approach for nano–particle drag prediction in the literature.

A class of methods known as discrete velocity models (DVM) [25, 26, 27] exist that have much in common with the LBM. Succi [28] provides a comparison of the LBM and DVM pointing out that even though they are close relatives in mathematical terms (since they are both based on grid–bound particles moving with a set of discrete speeds), the DVM remains more faithful to the underlying kinetic theory whereas the LBM is more concerned with 'capturing hydrodynamic phenomena', i.e. it is a more phenomenological methodology. There are molecular interaction 'simulation' methodologies that have been linked with the Boltzmann equation with sufficient rigour that they have been regarded as 'solutions' of the equation [29]. One such technique is the direct simulation Monte Carlo (DSMC) method pioneered by Bird [30]. In the strictest sense, the DSMC method is merely a phenomenological model, simulating the gas molecules rather than being derived from fundamental theory. The DSMC method is, however, extremely popular for simulating rarefied and highly non–equilibrium gas flows [31, 32, 33] because of its efficiency and parallelisability [34]. The method uses a probabilistic Monte Carlo approach in the tracking of simulation molecules, representing a large number of real molecules, through physical space and in the modelling of inter–molecular collisions and molecule–surface collisions.

A family of numerical schemes which may be generically described as 'kinetic schemes' exist [35, 36, 37, 38, 39, 40]that are designed specifically for the analysis of high Knudsen number flows. The method involves a Chapman–Enskog expansion analysis [41] of (usually) the Boltzmann–BGK equation to form a set of equations, similar in form to the Navier–Stokes equations, but including additional terms to account for the inter–molecular interactions and molecule–surface interactions. This removes the need for any kind of 'special' boundary treatment for high Knudsen number flows using the standard Navier–Stokes equations. One popular variant of such types of scheme is the Kinetic Flux Vector Splitting method [42, 43, 44]. This scheme employs a particular type of upwinding based on the flow physics at the Boltzmann level rather than the Euler/Navier–Stokes level. It is important to note that such methods are not direct solutions of the Boltzmann equation.

There are a limited number of direct numerical Boltzmann solvers detailed in the literature at the time of writing. Aristov [45] provides a general overview of discretisation approaches, especially focussing on the discretisation of velocity space. However, in physical space, he is limited to a finite difference approximation. Analysis of the literature on direct numerical approaches makes it clear that one of the principal difficulties in solution of the Boltzmann equation lies in the right–hand side collision term. A 'spectrally accurate approximation of the collision operator' is presented in [46] and [47]. In [48], a second order upwind finite difference scheme is applied to the simplified BGK and higher moment models of the Boltzmann equation. Other approaches to direct Boltzmann equation solution procedures do exist [49, 50, 51, 52] including a limited number of approaches [53, 54, 55, 56] involving a finite–element discretisation approach in physical space. In each of these cases the

application has been highly simplistic (and in most cases restricted to 1D) with no attempts (to the author's knowledge) to tackle the problem of nano–particle drag prediction.

The idea behind the approach presented in this paper was first outlined by Evans et al [57]. In this paper, the general methodology was applied to the collisionless form of the Boltzmann equation (valid for high Knudsen number flows) and used to analyse a rarefied shock tube example and rarefied subsonic flow over a vertical plate. This work was extended in [18] to include the BGK collision term in the formulation but applications were restricted to rarefied macroscopic gas flows. This paper presents the results from the first application of this method to nano–scale flows.

1.4. Alternative Solution Approaches

This section will briefly outline the solution approach that are being contrasted within this paper. For a more detailed description of the algorithms the reader is referred to [5, 13].

1.4.1. Molecular Dynamics

In a computational molecular dynamics approach, the physical movements of atoms and molecules are simulated and is thus a type of 'N-body' simulation. Atoms and/or molecules are allowed to interact for a fixed period of time, based on clearly defined interaction laws, giving a view of the dynamical evolution of the system. In the most common version, the trajectories of simulated particles are determined numerically using Newton's equations of motion in which the inter–particle forces are determined based on interatomic potentials or molecular mechanics force fields.

1.4.2. Modified Boundary Condition Continuum Approach

As the Knudsen number of a flow field is increased through the transition region ($Kn = 0.01 - 0.1$) the first difference that is noticed between continuum solutions and molecular level solutions is the behaviour of the flow field near solid boundaries. The traditional 'no slip' wall boundary condition is observed to break down and therefore attempts have been made [13, 15, 16] to model transitional flows with a continuum solver by simply modifying the wall boundary condition to match observations in flows at various higher Knudsen numbers. For more information on such approaches the reader is directed to an overview of Navier–Stokes based transitional modelling approaches in [17].

2. Boltzmann-BGK Discontinuous–Galerkin Finite Element Solution Approach

2.1. Physical and Velocity Space Discretisation

The solution approach for the Boltzmann–BGK equation used in this work will be briefly explained in this section. For a full description of the algorithm derivation the reader is referred to [18].

As the single dependent variable, the velocity distribution function, in the Boltzmann–BGK equation is defined across both *physical space* and *velocity space* a suitable discretisation approach must be adopted for both domains. The two dimensional physical space domain, Ω_r, is discretised into an unstructured assembly of discontinuous, linear, triangular elements with nodes at the vertices as shown in Figure 3. A discontinuous discretisation approach was chosen in order to naturally capture solution discontinuities such as shock waves.

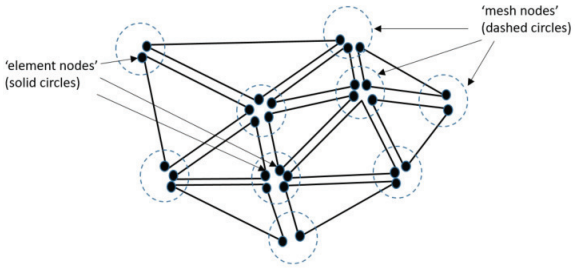

Figure 3: Physical space discretisation using an assembly of discontinuous, unstructured, triangular elements

The corresponding two dimensional velocity space domain, Ω_c, is, in principle, infinite in extent i.e. there is no natural limitation on the maximum speed of a molecule. However a finite limit, r_v, must be placed on the radial extent of the domain. The guide that was used on this limit in this work is that the limit of the velocity space should be several times larger than the mean thermal (peculiar) molecular velocity [30]. The assumption underpinning this guide is that the number (or fraction) of molecules travelling with a molecular speed higher than this cutoff limit have a negligible effect on the bulk properties of the flow. The validity of this assumption was tested in the previous work using the Boltzmann–BGK approach for studying high Kn macroscale flows [18]. This is justified when the molecular distribution functions are plotted (in Figures 17 - 19 in Section 3.2). These show the the product nf tails off rapidly towards zero as the magnitude of the molecular velocity increases beyond one or two thermal velocities. The velocity space domain description is shown in Figure 4.

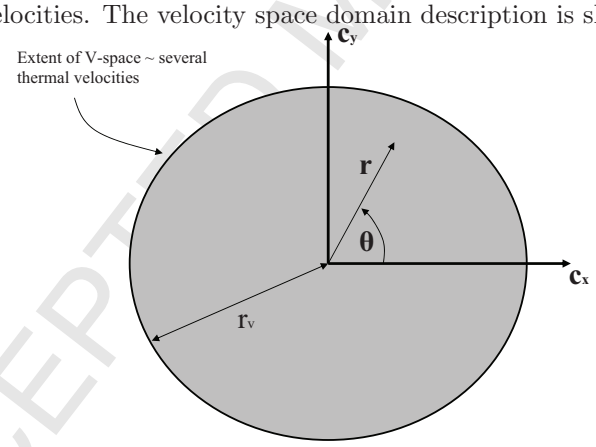

Figure 4: Velocity Space Domain

As the velocity space domain contains no internal geometries it can be discretised as a single high order (spectral) element. This is advantageous for efficient integration over the domain. It is convenient to map the domain from polar coordinates in real space into a quadrilateral element in the (η, ζ) plane, shown in Figure 5, using the transformation

$$\eta = \frac{2r}{r_v} - 1$$
$$\zeta = \frac{\theta}{\pi} \tag{6}$$

where (r, θ) are polar coordinates in real v–space and r_v is the radius of the v–space domain, i.e. the maximum molecular speed. A high order quadrature method is then applied to the element. In the η direction, a Lobatto quadrature is applied whereas in the ζ direction a constant spacing / constant weighting discretisation is applied. This results in a rotationally symmetric distribution of sampling points with no preferred radial direction, when the points are mapped back into real space. The coordinates of the quadrature points and the associated weightings in the (η, ζ) plane are shown in Figure 6 for a (20 x 20) discretisation. If these points are then mapped back into real space, the (u, v) plane, the corresponding coordinates and weights are as shown in Figure 7.

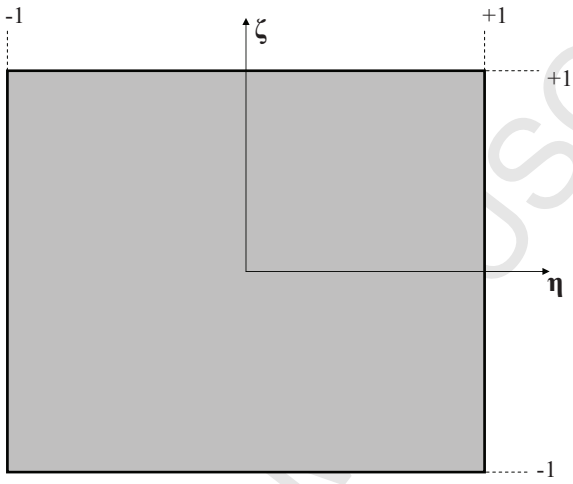

Figure 5: A Standard Quadrilateral Element in the (η, ζ) Plane

2.1.1. Equation Discretisation

A two–step discontinuous Taylor–Galerkin [63, 64] approach is implemented taking advantage of the approximation

$$(nf)_i^{m+\frac{1}{2}} = (nf)_i^m + (\frac{\Delta t}{2})Q^m - \frac{\Delta t}{2} c_i \frac{\partial (nf)_j}{\partial r_j}\Big|^m \tag{7}$$

where Q is computed as $Q = \nu(\boldsymbol{r}, t)((nf_0) - (nf))$ with f_0 representing the Maxwellian equilibrium distribution function, given in equation (5), modified to its two dimensional form, $f_0(\boldsymbol{c}) = \left(\beta^2/\pi\right) exp(-\beta^2(\boldsymbol{c} - \boldsymbol{c_0})^2)$ and ν is the molecular collision frequency determined as

$$\nu(\boldsymbol{r}, t) = \int_{-\infty}^{+\infty} \sigma_T |\boldsymbol{c} - \boldsymbol{c_1}| f \, d\boldsymbol{c_1} \tag{8}$$

where σ_T is the total collision cross section [30]. If we make the assumption of hard sphere molecules, we obtain the simplest possible expression for the total collision cross section, $\sigma_T = \pi d^2$, where d is the molecular diameter.

Step 1

A piecewise–constant increment $\Delta(nf)_{re,\boldsymbol{c}}$ is computed on each physical space element according to

$$\Delta(nf)_{re,\boldsymbol{c}} = \frac{\Delta t}{2} \Sigma Q^m_{k,\boldsymbol{c}} N_k - \frac{\Delta t}{2} F^m_{ik} \frac{\partial N_k}{\partial r_i}\Big]_{re,\boldsymbol{c}} \tag{9}$$

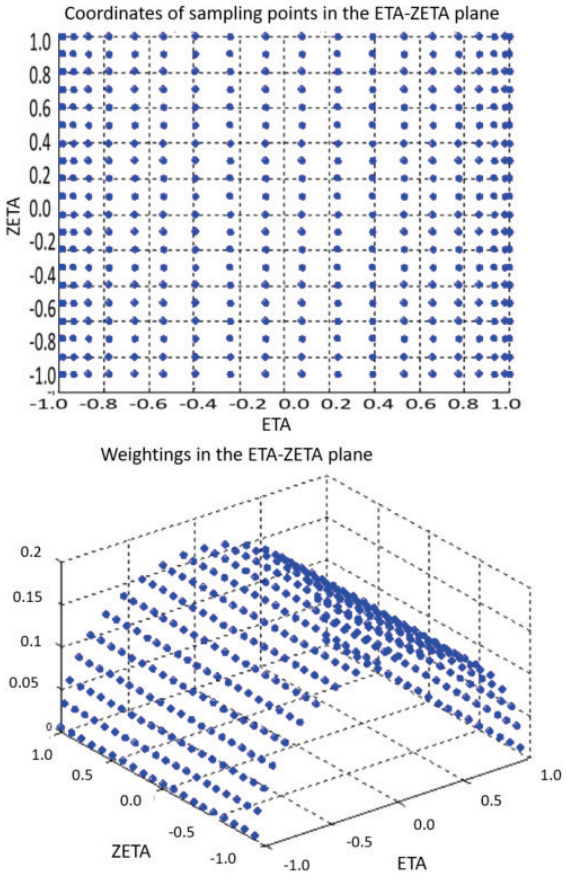

Figure 6: Quadrature Coordinates and Weights in the (η, ζ) Plane

where the summation k extends over the three nodes of element re, Δt is the global timestep governed by the Courant stability condition [18]. N_k is the standard, piecewise–linear finite element shape function associated with node k in physical space and

$$F^m_{ik,\boldsymbol{c}} = F_i\left((nf)^m_{k,\boldsymbol{c}}\right) = \boldsymbol{c}(nf)^m_{k,\boldsymbol{c}}. \tag{10}$$

The element fluxes at the half–timestep are then approximated by the piecewise linear discontinuous representation

$$F_i^{m+\frac{1}{2}}]_{re,\boldsymbol{c}} = F_i((nf)^m_{k,\boldsymbol{c}} + \Delta(nf)_{re,\boldsymbol{c}})N_k. \tag{11}$$

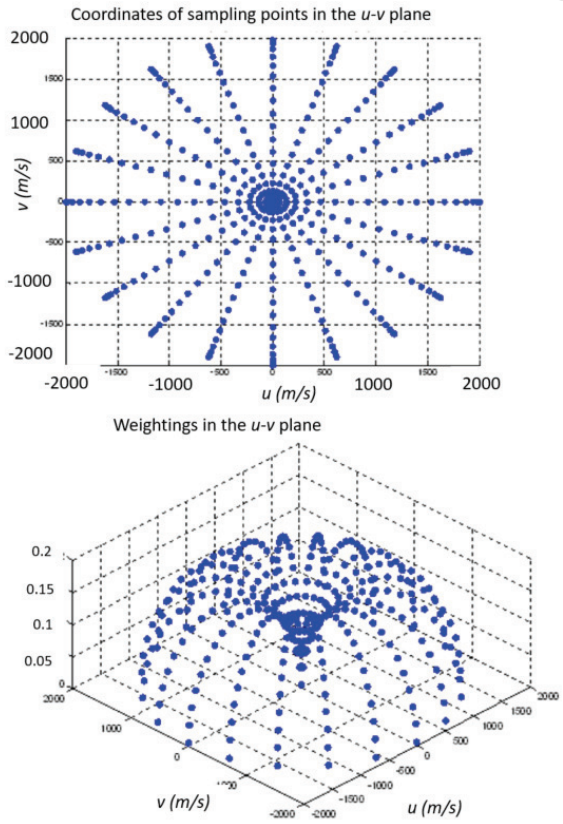

Figure 7: Quadrature Coordinates and Weights in the (u, v) Plane

Second Step

A piecewise–linear approximation for $\Delta(nf)$ on each physical space element is assumed which is discontinuous at the element edges. The element nodal values of the solution increment over the complete timestep are determined according to

$$M_L]_{re}\Delta(nf)_{k,\boldsymbol{c}} = \Delta t M_L]_{re} Q^{m+\frac{1}{2}} + \Delta t \int_{\Gamma_{re}} F_{n,\boldsymbol{c}}^{m+\frac{1}{2}} N_k \mathrm{d}\Gamma_{re} - \Delta t \int_{\Omega_{re}} F_{ik,\boldsymbol{c}}^{m+\frac{1}{2}} \frac{\partial N_k}{\partial r_i} \mathrm{d}\Omega_{re,\boldsymbol{c}} \tag{12}$$

where $M_L]_{re}$ is the standard, lumped, 3x3 physical space element mass matrix, $F_{n,\boldsymbol{c}}^{m+\frac{1}{2}}$ denotes the normal component of the upstream flux at the physical space element edges for a velocity of $\boldsymbol{c}$, Γ_{re} is the physical space element boundary and Ω_{re} is the physical space element domain.

For inter–element edges, the direction of the flux across the edge must be calculated based on the convection velocity. The convection velocity is determined by the v–space mesh node under consideration. If the flux is 'into the element', the integral in the first term on the RHS of (12) is given a value based on the corresponding upstream element edge flux. If the flux is 'out of the element', the same term is given a negative value based on the normal edge flux at that edge in the element. This ensures the local conservativeness of the scheme, since the fluxes of the distribution function are transferred directly from one element to the next.

In the BGK formulation shown here, the term ν is regarded as a collision frequency term and governs the rate at which the distribution function is restored to equilibrium. The form of the BGK collision term is such that the distribution function will be restored to equilibrium in a timescale,

$$\tau = O(\frac{1}{\nu}). \tag{13}$$

This places a further restriction on the allowable timestep size

$$\Delta t < \frac{1}{\nu}. \tag{14}$$

in addition to the Courant condition. Note that the Courant condition is dictated by the maximum molecular speed in the velocity space discetisation and therefore the choice of velocity space limit can affect the timestep used. In future work it might be possible to study the most effective velocity space limit for a given problem which maximises the allowable timestep size for a given solution accuracy but that was deemed beyond the scope of this work.

2.1.2. Boundary Condition Application

There are a range of potential approaches to deal with boundaries in the context of solution of the Boltzmann equation as detailed in the literature [65, 66, 67]. In this work application of the boundary conditions in the algorithm is achieved by an appropriate modelling of $F_{n,\boldsymbol{c}}^{m+\frac{1}{2}}$ in the first term on the right-hand side of equation 12. Essentially three types of boundary need to be considered; inflow, outflow and wall. Note that a more extensive discussion of the boundary condition implementation can be found in [18].

Inflow

The assumption is made that the gas flow entering the physical space domain is in thermodynamic equilibrium with prescribed macroscopic properties. As such, for molecular velocities directed into the physical space domain at an inflow boundary the inter–element flux is constructed as

$$F_{n,\boldsymbol{c}}^{m+\frac{1}{2}} = \boldsymbol{c}.\boldsymbol{n}(\frac{\beta^2}{\pi})\exp(-\beta^2(\boldsymbol{c}-\boldsymbol{c_o})). \tag{15}$$

$(\beta^2/\pi)\exp(-\beta^2(\boldsymbol{c}-\boldsymbol{c_o}))$ is the Maxwellian distribution function in two dimensions. If the molecular velocity is directed out of the physcial space domain the flux is computed as usual according to equation 10.

Outflow

At a physical space domain boundary flagged as an outflow the assumption is made that the gradient of macroscopic variables is zero perpendicular to the boundary and that the underlying molecular velocity distribution function is constant across the boundary. Therefore fluxes both into and out of the domain are constructed based on values inside the domain. This approach requires that outflow boundaries are positioned sufficiently far downstream for any unwanted reflection effects to be negligible.

Wall

At a wall the condition that must be enforced is zero mass flux across the boundary. In a molecular kinetic theory description this is expressed as

$$\int_{\Gamma_r}\int_{-\infty}^{+\infty} F_{n,\boldsymbol{c}}\,\mathrm{d}\boldsymbol{c}\,\mathrm{d}\Gamma_r = 0 \tag{16}$$

where $F_{n,\boldsymbol{c}} = (\boldsymbol{c}.\boldsymbol{n})f(\boldsymbol{c},\boldsymbol{r},t)$ and Γ_r is the section of the p–space domain boundary across which we wish to enforce zero mass flux. This condition is ensured by an appropriate modelling of molecular collisions with the wall. We make the assumption that a certain fraction, α, of molecules are absorbed by the wall and remitted in equilibrium with wall, i.e. they are reflected back into the domain with a Maxwellian distribution based on the wall temperature. This is termed diffuse reflection. The remaining fraction, $(1-\alpha)$, are not absorbed by the wall and simply reflect directly back into the domain. This is termed specular reflection. These two models, for the interaction of a flux of molecules with a solid surface, was first suggested by Maxwell [68]. The term α is referred to as the 'absorption coefficient' in this work and is analagous to the 'wall roughness parameter' used in molecular dynamics simulations [5]. It will be shown that this parameter has a powerful effect on the predicted flowfields (and therefore particle drag) under the conditions simulated.

The distribution function of the net reflected flux of molecules is, therefore, constructed as

$$f(\boldsymbol{c},\boldsymbol{r},t) = (1-\alpha)Rf(\boldsymbol{c},\boldsymbol{r},t) + \alpha Mf(\boldsymbol{c},\boldsymbol{r},t), \qquad \text{for} \quad \boldsymbol{c}.\boldsymbol{n} \leq 0 \tag{17}$$

where

$$Rf(\boldsymbol{c},\boldsymbol{r},t) = f(\boldsymbol{c}-2\boldsymbol{n}(\boldsymbol{n}.\boldsymbol{c}),\boldsymbol{r},t) \tag{18}$$

$$Mf(\boldsymbol{c},\boldsymbol{r},t) = \eta(\boldsymbol{r},t)M_w(\boldsymbol{c}) \tag{19}$$

and $\boldsymbol{n}$ is the outward facing unit normal at the wall. If T_w is the wall temperature and R is the gas constant, then M_w is determined as

$$M_w = \exp(-\frac{c^2}{2\,R\,T_w}) \tag{20}$$

The parameter η is used to enforce the zero perpendicular mass flux condition using the method outlined in [18].

2.1.3. Post–processing for macroscopic variables

Given that the dependent variable f is a probability distribution function for the molecular speed, at each point in physical space the mean value of any molecular quantity, Q, is defined as

$$\overline{Q} = \int_{-\infty}^{\infty} Q f(\boldsymbol{c})\, \mathrm{d}\boldsymbol{c}. \tag{21}$$

By setting Q to the appropriate molecular quantity, we can obtain the macroscopic properties as follows:

-density ρ: $Q = m$ where m is the molecular mass

-bulk velocity $\boldsymbol{v_i}$: $Q = \boldsymbol{c_i}$

-static pressure p_i: $Q = mc_i'^2$ where $\boldsymbol{c_i'} = \boldsymbol{c_i} - \boldsymbol{v_i}$ (thermal / peculiar velocity) To determine the temperature, we simply use the definition of kinetic temperature,

$$T_k = \frac{p}{R\rho}. \tag{22}$$

We evaluate the integral in equation (21) by transforming the coordinate system from the real v–space coordinates to the (η, ζ) plane. Moving from Cartesian to polar coordinates gives us

$$\begin{aligned} u = r\cos\theta \quad &\Rightarrow \quad \frac{\partial u}{\partial r} = \cos\theta, \frac{\partial u}{\partial \theta} = -r\sin\theta \\ v = r\sin\theta \quad &\Rightarrow \quad \frac{\partial v}{\partial r} = \sin\theta, \frac{\partial v}{\partial \theta} = r\cos\theta. \end{aligned} \tag{23}$$

The Jacobian, J, of the transformation from Cartesian to polar coordinates is, therefore,

$$|J| = \begin{vmatrix} \dfrac{\partial u}{\partial r} & \dfrac{\partial u}{\partial \theta} \\ \dfrac{\partial v}{\partial r} & \dfrac{\partial v}{\partial \theta} \end{vmatrix} = r\cos^2\theta + r\sin^2\theta = r \tag{24}$$

so that

$$\overline{Q} = \int_{-\infty}^{\infty} Q f(\boldsymbol{c})\, \mathrm{d}\boldsymbol{c} \Rightarrow \int_{-\pi}^{+\pi} \int_{0}^{r_v} Q f(r,\theta)\, r\, \mathrm{d}r\, \mathrm{d}\theta. \tag{25}$$

The mapping from the real polar v–space to the (η, ζ) plane gives

$$\begin{aligned} r = \frac{r_v}{2}(\eta + 1) \quad &\Rightarrow \quad \frac{\partial r}{\partial \eta} = \frac{r_v}{2}, \frac{\partial r}{\partial \zeta} = 0 \\ \theta = \zeta\pi \quad &\Rightarrow \quad \frac{\partial \theta}{\partial \eta} = 0, \frac{\partial \theta}{\partial \zeta} = \pi \end{aligned} \tag{26}$$

so that the Jacobian, J, of the transformation is

$$|J| = \begin{vmatrix} \dfrac{\partial r}{\partial \eta} & \dfrac{\partial r}{\partial \zeta} \\ \dfrac{\partial \theta}{\partial \eta} & \dfrac{\partial \theta}{\partial \zeta} \end{vmatrix} = \begin{vmatrix} \dfrac{r_v}{2} & 0 \\ 0 & \pi \end{vmatrix} = \frac{\pi r_v}{2}. \tag{27}$$

We can rewrite equation (25) as

$$\overline{Q} = \int_{-1}^{+1} \int_{-1}^{+1} Q f(\eta, \zeta) \frac{\pi r_v^2}{4} (\eta + 1)\, \mathrm{d}\eta\, \mathrm{d}\zeta \tag{28}$$

so that the integral in equation (21) may be evaluated using the high order quadrature method as

$$\overline{Q} = \frac{\sum_{i=1}^{N} w_i Q(nf)_i |J|}{\sum_{i=1}^{N} w_i (nf)_i |J|} \tag{29}$$

where the summations are over all the v–space sampling points in the discretisation, w_i is the weighting associated with the point and $|J| = \frac{\pi r_v^2}{4}(\eta_i + 1)$.

The macroscopic variables are calculated at the element nodes. For post–processing of the results, data defined at the mesh nodes is required. This is achieved using the simple element weighted averaging procedure.

$$\overline{Q_m} = \frac{\sum_{i=1}^{n} A_i \overline{Q_i}}{\sum_{i=1}^{n} A_i} \tag{30}$$

where $\overline{Q_m}$ is the value of the macroscopic variable at the mesh node, the summations are over each discontinuous node, i, meeting at the mesh node, A_i is the area of the element associated with discontinuous node i and $\overline{Q_i}$ is the value of the macroscopic variable at discontinuous node i.

2.1.4. Parallelisation

Due to the large memory requirement involved in discretising both physical and velocity space domains, parallelisation of the algorithm is required for realistic problems to be tackled (even in two dimensions). The code has therefore been parallelised via physical space domain decomposition utilising the METIS family of graph partitioning libraries [69]. For more details you are referred to [18].

3. Results

In this study, a set of 24 steady simulations was undertaken at a range of Re between 0.25 and 2.0 (the conditions for this set of simulations is summarised in Table 1). The details of the particle geometry under consideration is shown in Figure 1. The channel was extended a distance of 10nm upstream and 20nm downstream in order to avoid unwanted reflection effects from the inflow and outflow boundaries. The bulk flow was considered travelling from left to right, relative to Figure 1 with standard inflow boundary conditions applied to the left-hand boundary and standard outflow boundary conditions applied to the right-hand boundary. All other boundaries (including that defining the particle) were considered to be solid walls. At each discrete Re considered, a simulation was run with the wall absorption parameter, α first set to 0.9 (as recommended in the literature for boundary conditions of this type for macroscopic flows [68]) and then modified to the upper limit of 1.0 (purely diffuse reflection) and lower limit of 0.0 (purely specular reflection) in order to analyse the effect of this parameter on the solution.

Following a phase space discretisation convergence study it was determined that a suitable physical space discretisation for this problem was as shown in Figure 8. This physical space mesh consists of 29,261 elements (3 x 29,261 = 87,783 discontinuous nodes). The velocity space mesh was disretised using 1,600 nodes resulting in total of 1,600 x 87,783 $\approx$ 140M degrees of freedom in the system. Each steady state simulation was run across 32 cores (distributed over 2 nodes) of an Intel Xeon Sandy Bridge based PC Cluster (utilising Infiniband interconnect). Convergence to 5 orders of magnitude reduction in the L2 (Euclidean) norm of nf across phase space (which equated to approximately 3 significant figure accuracy in the drag coefficient) took approximately 24hrs wallclock

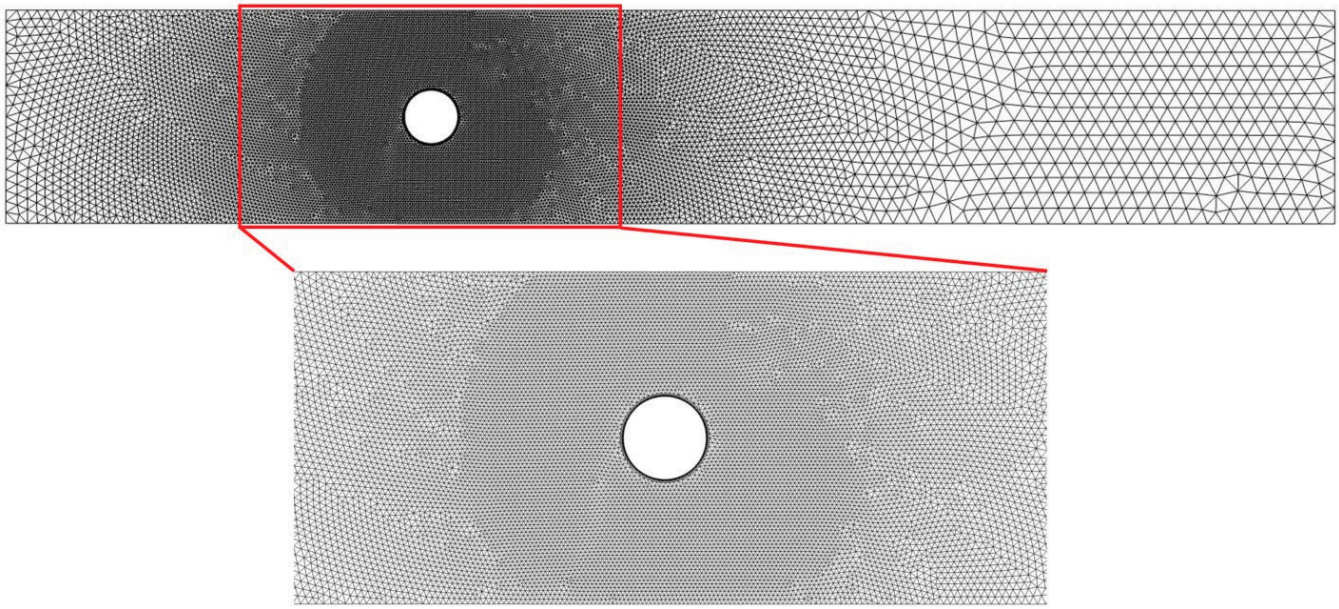

Figure 8: Unstructured triangular Physical space mesh used for simulations comprising 29,261 elements (87,783 discontinuous nodes). Note that 12 layers of quasi-structured (triangular) boundary layer mesh is utilised.

time. The problem set up and computational resource requirements for the simulations is summarised in Table 1.

3.1. Drag Prediction Comparison

Table 2 summarises the computed drag coefficient, C_d for each of the 24 simulations in this study. It is clear that at each α setting the predicted C_d reduces asymptotically with Re_∞. Also, as you might expect, the $\alpha = 1.0$ C_d values are much closer to the $\alpha = 0.9$ values than the $\alpha = 0$ results. It is also clear already that the α setting has a significant impact on the predicted drag. Given that this parameter is analagous to the surface roughness parameter, f utilised in a molecular dynamics simulation approach, this is perhaps not surprising since the results of Hafezi et al [5] also indicate that predicted drag coefficients in this regime are highly dependent on f. The final row in Table 2 indicates the standard deviation of the three predictions of C_d at each Re_∞. Clearly the absolute dependence on α is tending to decrease with increasing Re_∞ (as the magnitude of C_d is also decreasing). In percentage terms the variation of C_d with α remains roughly constant.

Figure 9 shows the results from Table 2 plotted and compared with the molecular dynamics results of Hafezi [5] and Tang [14] and results from the modified continuum approach of Lagree [13]. The solid line indicates the results from the finite element Boltzmann–BGK solver (this work) with $\alpha = 0.9$ (since this was the a priori assumption on the most suitable setting for α) with the error bars indicating the range of solutions possible over the α range 0.0 (lower) to 1.0 (upper). The two dashed lines show the solutions of Hafezi with $f = 0$ (lower) and $f = 1$ (upper), the dotted line indicates the continuum predictions of Lagree and the 'dot-dash' line indicates the molecular dynamics solution of Tang under the same conditions but with Argon gas modelled (rather than Methane). Clearly, given the range of discrepancy in existing solutions to this problem (and absence

Parameter	Value
Kn_∞	0.0214
Re_∞	0.25, 0.5, 0.75, 1.0, 1.25, 1.5, 1.75, 2.0
Gas	Methane
Gas constant, R	518 J/Kg K
Molecular diameter, d	414e-12m
Molar mass, M	16g
Geometry	2nm diameter circular particle, 8.2nm wide channel
p-space mesh	29,261 elements (87,783 discontinuous nodes)
v-space mesh	16,000 nodes
DoFs	140 million
r_v	2,000 m/s
α	0.0,0.9,1.0
compute	32 cores
No. timesteps	$\approx$ 150,000 to converge (3sf drag)
wallclock runtime	24hrs

Table 1: Summary of simulation conditions and computational requirements

Kn_∞ 0.0214								
	Re_∞							
α	0.25	0.5	0.75	1.0	1.25	1.5	1.75	2.0
0.9	182	110	65	45.9	30.2	25.5	24.7	23.1
0.0	104	57.1	32.3	21.1	15.9	13.2	12.6	10.1
1.0	186	120	75.5	48.6	32.1	26.2	24.8	23.5
Stand. Dev.	37.9	27.6	18.4	12.4	7.6	5.9	5.7	6.3

Table 2: Drag coefficient, C_d results summary showing the variation in drag prediction with Re and α. Note that the standard deviation is based on the three α settings considered at each Re.

of experimental data or analytical solutions) the direct Boltzmann–BGK solution approach provides remarkably consistent predictions, most closely aligned with the molecular dynamics results of Hafezi et al. However, it must be noted that the direct Boltzmann–BGK solution approach presented here is more computationally expensive than the molecular dynamics approach of Hafezi whose simulations converged to steady state in a similar timeframe but parallelised across only 8 cores.

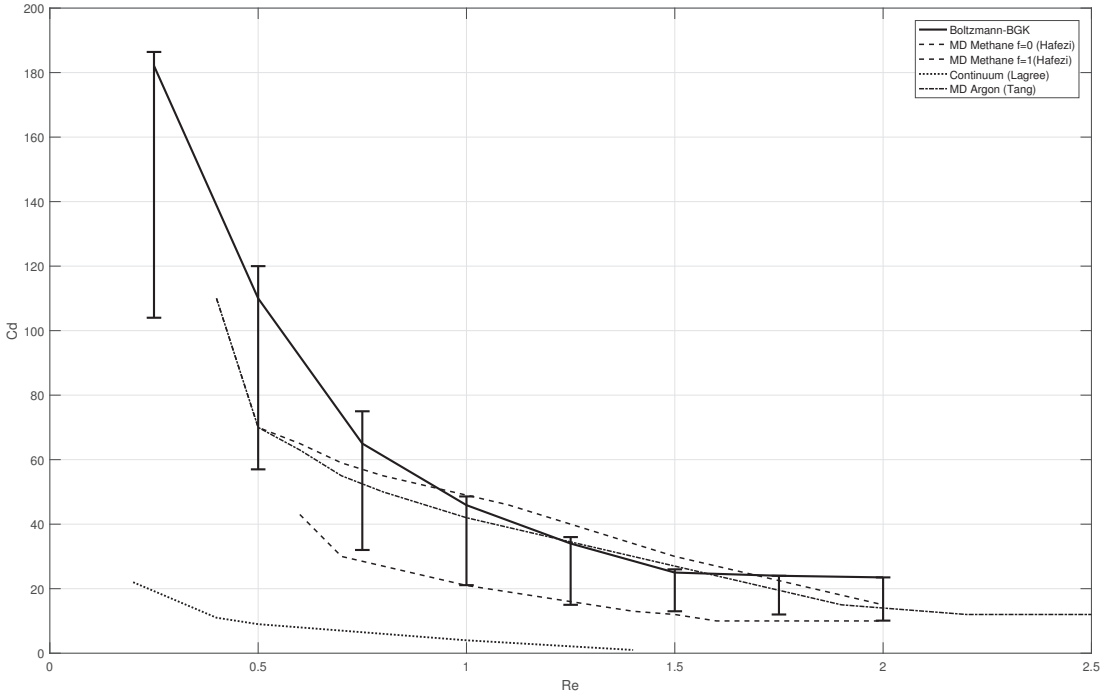

Figure 9: Drag coefficient, C_d prediction comparisons

3.2. Flowfield Analysis

Three discrete Re values were chosen ($Re = 0.25, 1.0, 2.0$) in order to study the predicted flowfields. Figures 10, 11 and 12 show the normalised pressure (p/p_∞) and normalised bulk flow speed ($|\mathbf{v}| \,/\, |\mathbf{v}|_\infty$) in the vicinity of the nano–particle. Note that only the $\alpha = 0.0$ and $\alpha = 0.9$ flow-fields are shown since the $\alpha = 1.0$ solutions were so similar to the $\alpha = 0.9$ solutions.

It is immediately evident that the wall absorption parameter, α has a dominating impact on the flowfield predictions (and hence the particle C_d values). The differences between the flowfield solutions with α appear to be highest at the lower Re_∞ considered. This observation seems to correlate with the findings of Hafezi et al [5] with reference to the impact of the wall roughness parameter, f. It is clear, particularly at higher Re_∞ that the effect of increasing α is similar to the impact of enforcing a the 'no slip' boundary conditions in a continuum solver. Given the definition of α (i.e. the percentage of molecules absorbed into the wall and remitted with

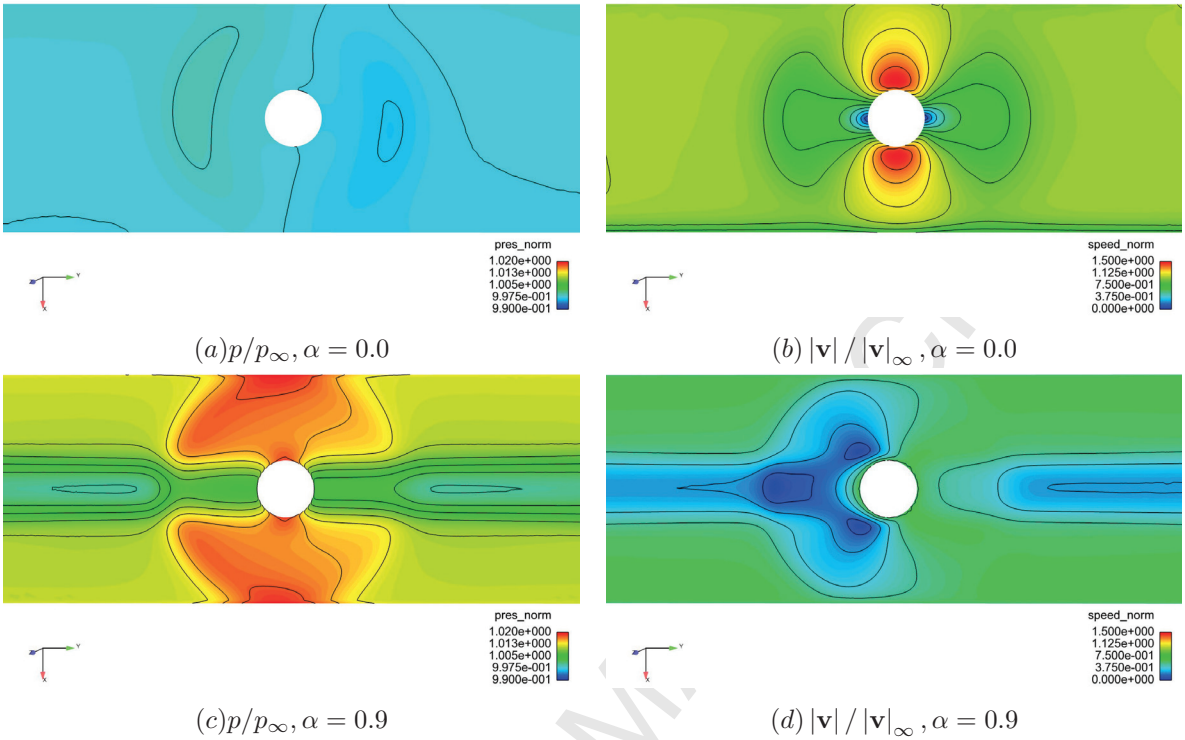

Figure 10: Predicted flow-field solutions at $Re_\infty = 0.25$ showing p/p_∞ and $|\mathbf{v}| \,/\, |\mathbf{v}|_\infty$ at $\alpha = 0.0$ ((a),(b)) and $\alpha = 0.9$ ((c),(d))

the thermal properties of the wall) this is to be expected. Given the dominance of the effect of α parameter on drag prediction at these small scale, low Re flows, this does beg the question of how one should make 'a priori' decisions on the appropriate setting for α for a given case. This is still a largely unanswered question since there is so little alternative analytical, empirical or numerical data to compare solutions to.

It is also interesting to note that at these low Re_∞ values the variations from freestream conditions in the velocity field are much larger than the deviations from freestream in the pressure field in all of the cases considered.

Figure 13 details the definitions of two lines (1234 and 5678) with 8 disrete coordinate points (1,2,3,4,5,6,7,8) at which the flowfield behaviour and underlying molecular behaviour has been analysed. These lines were chosen to allow comparison with the results of Hafezi et al [5].

Figures 14, 15 and 16 show the normalised (v_x,v_y) bulk velocity components along lines 1234 and 5678 (with reference to Figure 13. The solid line in these figures represents the $\alpha = 0.9$ solution, the dotted line represents the $\alpha = 0.0$ solution and the crosses represent the $\alpha = 1.0$ solution. It is evident that the percentage deviations in the bulk flow velocities from freestream values increase with Re_∞ as you might expect. It is also clear that the $\alpha = 0.9$ and $\alpha = 1.0$ solutions are very similar and at these high α settings enforce a no slip condition (or close to a no slip condition) at solid boundaries whereas the $\alpha = 0.0$ condition allows slip at the walls. This is particularly clear in the $v_x / |\mathbf{v}|_\infty$ ((a) and (c)) plots where the lines meet the horizontal boundary at the upper and lower extremes of the lines plotted where they meet the horizontal wall boundary of the channel. These

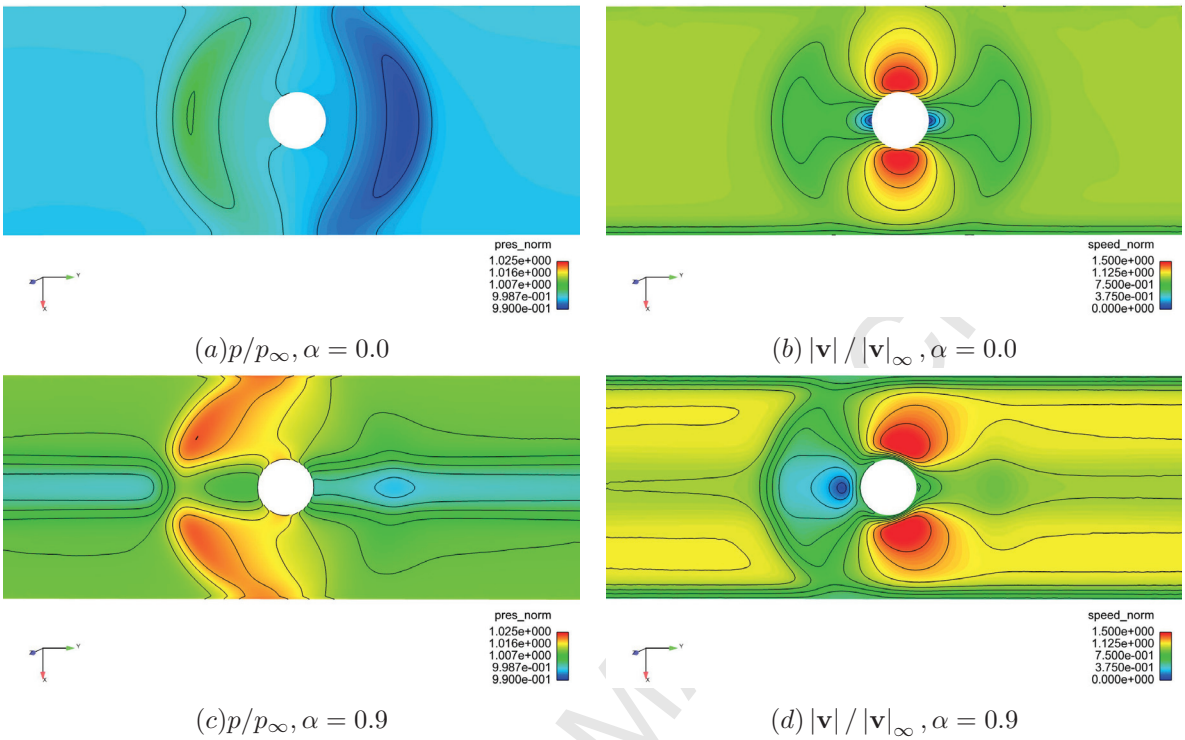

Figure 11: Predicted flowfield solutions at $Re_\infty = 1.0$ showing p/p_∞ and $|\mathbf{v}| \,/\, |\mathbf{v}|_\infty$ at $\alpha = 0.0$ ((a),(b)) and $\alpha = 0.9$ ((c),(d))

obervations compare qualitatively well with the observations of Hafezi et al.

Finally, the underlying molecular velocity distributions (which are captured at all points in physical space in a solution of the Boltzmann-BGK equation) were analysed at the disrete coordinates represented by the crosses 1,2,3,4,5,6,7,8 in Figure 13. These are shown in Figures 17 ($Re_\infty = 2.0, \alpha = 0.9$), 18 ($Re_\infty = 0.25, \alpha = 0.9$) and 19. Each figure shows the distribution of (nf) with molecular velocity (c_x, c_y). The obvious observation from these three figures is that the variations in the molecular distribution function from equilibrium (Maxwellian) are minor (almost unobservable) even though these minor departures from equilibrium are driving significant differences in the bulk flowfields that are directly derived as integrals across this velocity space. This observation does give confidence that the BGK approximation assumption used in this work (i.e. that departures from equilibrium are small) is valid in the cases considered.

4. Conclusions and Future Work

The work presented in this paper details the first ever attempt, to the author's knowledge, to study the flow and drag characteristics of a nano–scale particle by means of direct solution of the Boltzmann equation. The method utilised in this work is based on a discontinuous Galerkin finite element approach for physical space discretisation coupled to a spectral disretisation scheme for molecular velocity space. The problem of a 2D circular particle 2 nm in diameter within flow constrained by an 8.2 nm wide channel is considered at a transitional Knudsen number, Kn of 0.0214 and freestream Reynold's number, Re_∞ across the range 0.25 to

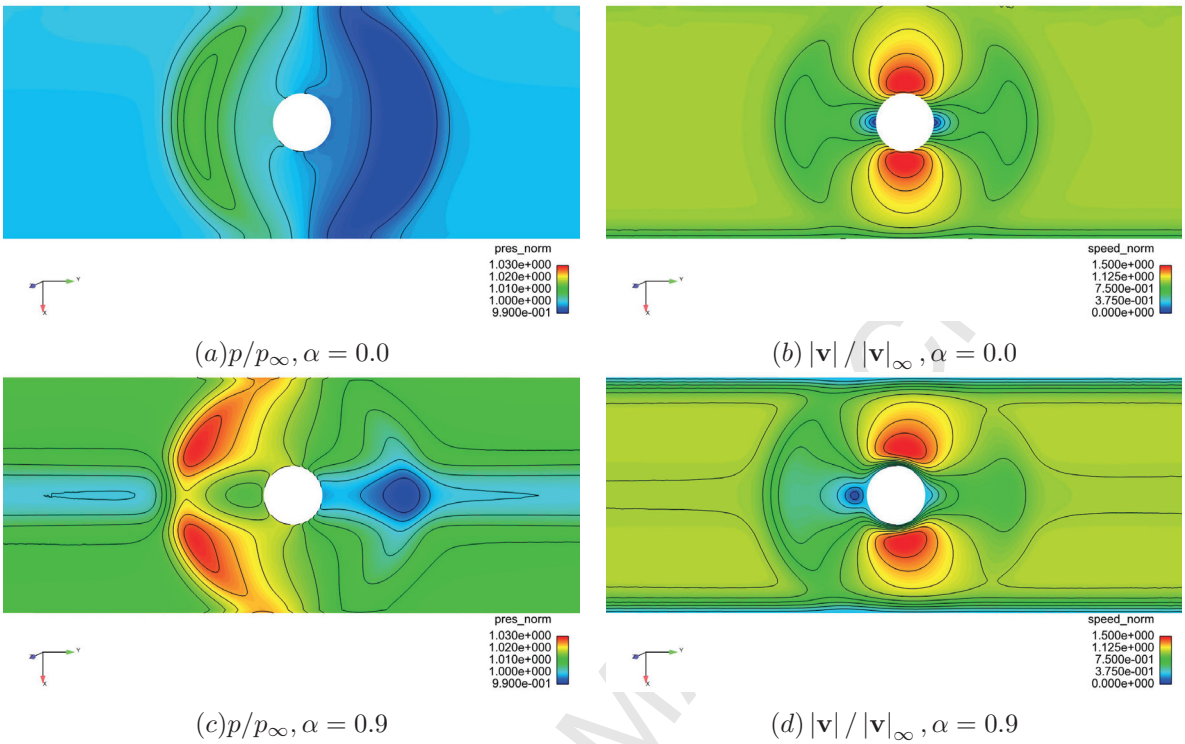

Figure 12: Predicted flowfield solutions at $Re_\infty = 2.0$ showing p/p_∞ and $|\mathbf{v}| \,/\, |\mathbf{v}|_\infty$ at $\alpha = 0.0$ ((a),(b)) and $\alpha = 0.9$ ((c),(d))

2.0. The results show that this method produces drag predictions that compare favourably with a range of other numerical approaches to the solution of this problem using molecular dynamics and modified continuum numerical schemes. The results indicate that the simulated flowfields and drag predictions are highly sensitive to the assumed wall absorption parameter applied at solid wall boundaries and variations in predicted drag to this parameter are similar to the variations in drag predicted when varying the wall roughness parameter in molecular dynamics simulations. There are a number of potential applications for solvers such as this in nano–scale fluidics ranging from therapeutic and diagnostic bio–medical applications to applications in the semiconductor and xerographic fields.

A review of the literature and the work presented in this paper indicate that the field of nano–fluidic flowfield modelling is still in its infancy. The approach outlined in this paper adds to the growing body of work that is generating solutions to nano–particle drag prediction. It is hoped that in the future an increased understanding (and experimental data) for such applications will allow these techniques to be improved. As part of ongoing work it is also hoped that the inclusion chemical forces within the scheme will be developed to widen the range of problems that can be tackled. One important improvement to the Boltzmann–BGK solver outlined in this work that will also be implemented in future work is an improvement to the parallelisation approach to incorporate both physical and velocity space domain decomposition. This should improve the computational efficiency of the scheme allowing more complex (and potentially 3D) geometries at this scale to be studied in the near future.

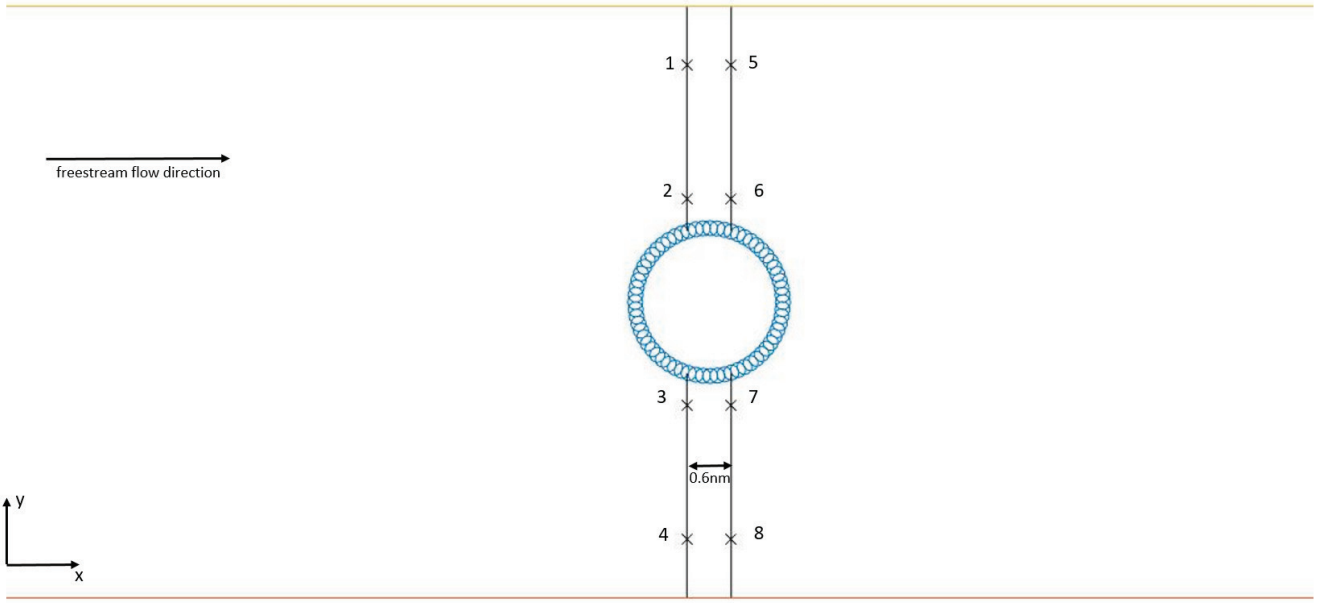

Figure 13: Definition of lines and coordinates used for results plotting

5. References

[1] Borisenko, VE, et al, Physics, Chemistry and Applications of Nanostructures - Proceedings of International Conference Nanomeeting, 2015

[2] Turgeon, ML., Clinical Haematology Theory and Procedures, Lippincott Williams & Wilkins, 2005

[3] Berg, HCE., Coli in Motion, Springer–Verlag, New York, 2004

[4] Mandelkern, M., Elias, JG, Eden, G, Crothers, DM, The dimensions of DNA in solution, Journal of Molecular Biology, 152, 153–160, 1981

[5] F Hafezi, RS Ransing, RW Lewis, The calculation of drag on nano-cylinders, International Journal for Numerical Methods in Engineering, 2016

[6] Bawa R. Nanoparticle-based Therapeutics in Humans: A Survey. Nanotechnology Law & Business, 5, 135–155, 2008.

[7] Groneberg DA, Rabe KF & Fischer A., Novel concepts of neuropeptide-based drug therapy: Vasoactive intestinal polypeptide and its receptors. European Journal of Pharmacology 533, 182-194, 2006

[8] Couvreur P., Nanoparticles in drug delivery:Past, present and future, Advanced Drug Delivery Reviews, 65, 21–23, 2013

[9] Kingsley JD, Dou H, Morehead J, Rabinow B, Gendelman HE & Destache CJ. Nanotechnology: a focus on nanoparticles as a drug delivery system. J Neuroimmune Pharmacol 2006; 1, 340-50

[10] Uhrich KE, Cannizzaro SM, Langer RS & Shakesheff KM. Polymeric systems for controlled drug release. Chem Rev 1999; 99, 3181-98

[11] Ahmadi G., Guo S. Bumpy Particle Adhesion and Removal in Turbulent Flows Including Electrostatic and Capillary Forces. The Journal of Adhesion 2007; 83, 289-311

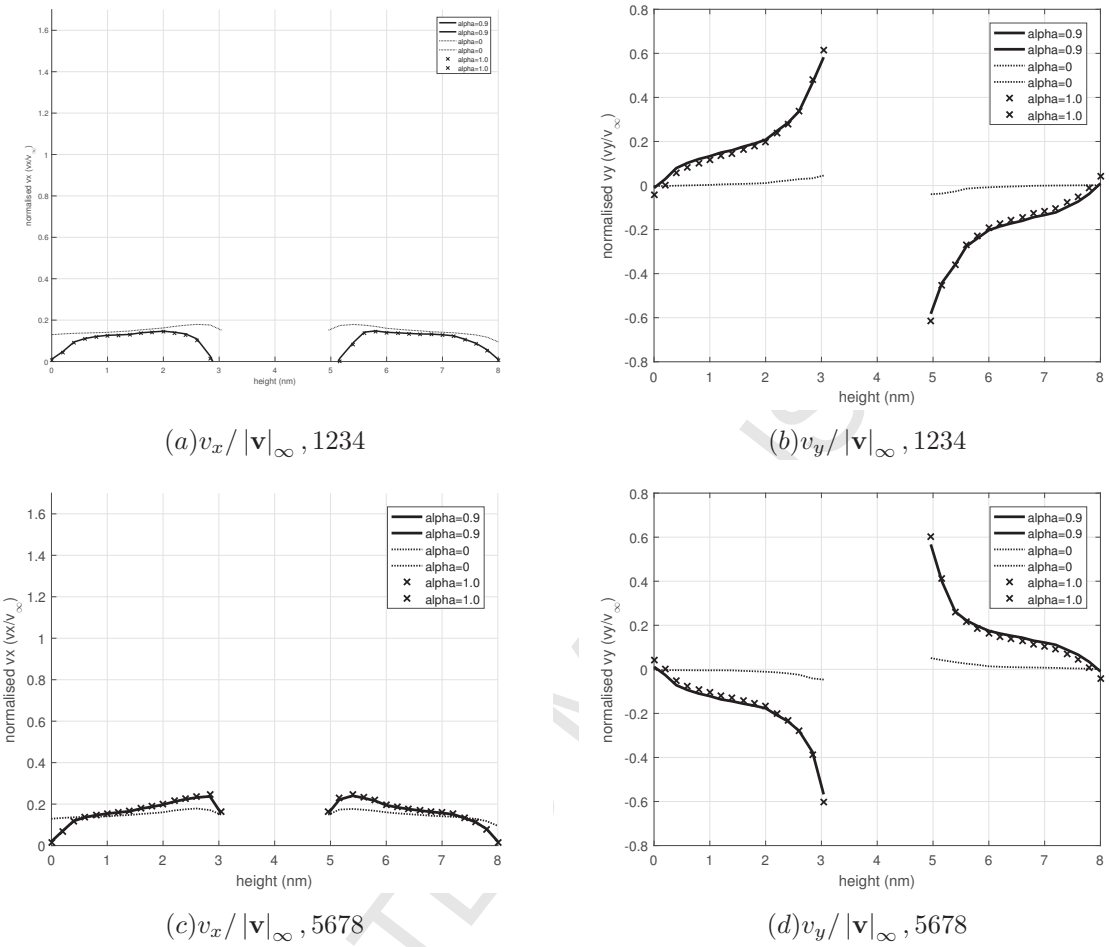

$(a) v_x/\left|\mathbf{v}\right|_\infty, 1234$ $(b) v_y/\left|\mathbf{v}\right|_\infty, 1234$

$(c) v_x/\left|\mathbf{v}\right|_\infty, 5678$ $(d) v_y/\left|\mathbf{v}\right|_\infty, 5678$

Figure 14: $Re_\infty = 0.25$ bulk velocity (v_x and v_y component) distributions at $\alpha = 0.0, 0.9, 1.0$ on lines 1234 ((a),(b)) and 5678 ((c),(d))

[12] Huang C, Choi PY, Nandakumar K. & Kostiuk LW. Investigation of entrance and exit effects on liquid transport through a cylindrical nanopore. Phys Chem Chem Phys 2008; 10, 186-92

[13] Lagree, P. Y. Small Re flows [Online]. Paris: Institut Jean Le Rond Alembert, 2013. Available: http://www.lmm.jussieu.fr/ lagree/COURS/M2MHP/petitRe.pdf [Accessed 8th March 2017]

[14] Tang W and Advani S.G. Drag on nanotube in uniform liquid argon flow. The Journal of Chemical Physics 2006; 125, 174706

[15] Maurer, J., Tabeling, P., Joseph, P. & Willaime, H., Second-order slip laws in microchannels for helium and nitrogen, Physics of Fluids 15, 2613-2621 (2003)

[16] Dongari, N. & Agrawal, A., Modeling of Navier–Stokes equations for high Knudsen number gas flows, International Journal of Heat and Mass Transfer 55, 4352-4358 (2012)

[17] Sturnfield, J., Understanding the Transitional Flow region through COMSOL Multiphysics modelling. Available: www.comsol.com/paper/download/257821/sturnfield_presentation.pdf

[18] B. Evans, K. Morgan, O. Hassan, A discontinuous finite element solution of the Boltzmann kinetic equation in collisionless and BGK forms for macroscopic gas flows, *Applied Mathematical Modelling*, **35**, 996–1015, 2011

[19] S. Chen G.D. Doolen, Lattice Boltzmann method for fluid flows, Annu. Rev. Fluid Mech., 30, 329–364, 2001

[20] N. Rossi S. Ulbertini G. Bella S. Succi, Unstructured lattice Boltzmann method in three dimensions, Int. J. for Numer. Meth. Fluids, 49, 619–633, 2005

[21] D. Yu R. Mei W.Shyy,Improved treatment of the open boundary in the Lattice Boltzmann equation, Prog. Comp. Fluid Dyn., 5 (1/2), 3–12, 2005

[22] Y. Xuan K. Yu Q. Li, Investigation on flow and heat transfer of nanofluids by the thermal Lattice Boltzmann model, Prog. Comp. Fluid Dyn., 5 (1/2), 13–19, 2005

[23] B. Shi N. He N. Wang, A unified thermal Lattice BGK model for Boussinesq equations, Prog Comput Fluid Dyn, 5 (1/2), 50–64, 2005

[24] H. Li X. Lu H. Fang Z. Lin, Simulation of multi-particle suspensions in a quasi-two-dimensional symmetric stenoic artery with Lattice Boltzmann method, Prog. Comp. Fluid Dyn., 5 (1/2), 65–74, 2005

[25] L. Mieussens, Discrete-Velocity Models and Numerical Schemes for the Boltzmann-BGK Equation in Plane and Axisymmetric Geometries, J. Comp. Phys., 162, 429–426, 2000

[26] R. Illner W. Wagner, A Random Discrete Velocity Model and Approximation of the Boltzmann Equation, J. Stat Phys., 70 (3/4), 773–792, 1993

[27] A. Palczewski J. Schneider A.V. Bobylev, A consistency result for a discrete-velocity model of the Boltzmann equation, SIAM J. Numer. Anal., 34 (5), 1865–1883, 1997

[28] S. Succi, The Lattice Boltzmann Equation for Fluid Dynamics and Beyond, Oxford University Press, Oxford, pp 72, 2001

[29] L. Pareschi S. Trazz, Numerical Solution of the Boltzmann equation by time reed Monte Carlo (TRMC) methods, Int. J. Numer. Meth. Fluids., 48, 947–983, 2005

[30] G.A. Bird, Molecular Gas Dynamics and the Direct Simulation of Gas Flows, Clarendon Press, Oxford, 1994

[31] L. Pareschi R.E. Caflisch, An Implicit Monte Carlo Method for Rarefied Gas Dynamics, J. Comp. Phys., 154, 90–116, 1999

[32] E.P. Muntz, Rarefied Gas Dynamics, Annual Rev. Fluid Mech., 21,PP 387, 1989

[33] D.I. Pullin, Direct Simulation methods for compressible inviscid ideal gas flow, J. Comput. Phys., 34, 231–244, 1978

[34] J.-S. Wu K.-C. Tseng, Parallel DSMC method using dynamic domain decomposition,Int. J. Num. Meth. Eng, 63, 37–76, 2005

[35] G. May A. Jameson, Improved Gas kinetic Multigrid Method for Three-Dimensional Computation of Viscous Flow, 17th AIAA Computational Fluid Dynamics Conference, Toronto, 1–18, 2005

[36] C.E. Siewert D. Valougeorgis, The temperature-jump problem for a mixture of two gases, Journal of Quantitative Spectroscopy and Radiative Transfer, 70, 307–319, 2001

[37] Y. Ruan A. Jameson, Gas-Kinetic BGK Method for Three-Dimensional Compressible Flows, AIAA-2002-0550, 2002

[38] K. Xu M. Mao L. Tang, A multidimensional gas-kinetic BGK scheme for hypersonic viscous flow, J. omp. Phys., 203, 405–421, 2005C

[39] J. Reese M. Gallis D. Lockerby, New directions in fluid dynamics: non-equilibrium aerodynamic and microsystem flows, Phil. Trans. R. Soc. Lond. A, 361, 2967–2988, 1965

[40] C.K. Chu, Kinetic-Theoretic description of the formation of a shock wave, Physics of Fluids, 8, 12–22, 1965

[41] S. Chapman T.G. Cowling, The Mathematical Theory of Non-Uniform Gases, 3rd ed., Cambridge University Press,Cambridge , 1970

[42] S.M. Deshpande et. al. , A 3-dimensional upwind Euler solver using kinetic flux vector splitting method, Proceedings of 13th International Conference on Computaional Fluid Dynamics, 1992

[43] N.P. Weatherill J.S. Mathur M.J. Marchant, An Upwind Kinetic Flux Vector Splitting Method on General Mesh Topologies, Int. J. Num. Meth. Eng., 37, 623–643, 1994

[44] B. Khonalatte P. Leyland, New Finite-Element-Based Fluctuation Splitting Schemes, Int. J. Num. Meth. Eng., 27, 229–239, 1998

[45] V.V. Aristov, Direct Methods for Solving the Boltzmann Equation and Study of Nonequilibrium Flows, Kluwer Academic Publishers, Dordrecht, The Netherlands, 2001

[46] L. Pareschi G. Russo, Numerical Solution of the Boltzmann Equation I: Spectrally Accurate Approximation of the Collision Operator, SIAM J. Numer. Anal., 37, 1217–1245, 2000

[47] F.Filbet G. Russo, High order numerical methods for the space non-homogeneous Boltzmann equation, J. Comp. Phys., 186, 457–480, 2003

[48] N. Satofuka K. Morinishi T. Oishi, Numerical solution of the kinetic model equations for hypersonic flows, J. Comp. Mech., 11, 452–464, 1993

[49] E. Fatima F. Odeh, Upwind finite difference solution of Boltzmann equation applied to electron transport in semiconductor devices, J. Comput. Phys., 108, 209–217, 1993

[50] C. Ringhofer, Space-time discretization of series expansion methods for the Boltzmann transport equation, SIAM . Numer. Anal., 38 (2) , 442–465, 2000

[51] S.G. Webster M.K. Gobbert T.S. Cale, Transient 3D/3D transport and reactant-wafer interactions: Adsorption and desorption, Rapid Thermal and Other Short-Time Processing Technologies III, 11, 81–88, 2002

[52] Pieraccini,S., Puppo, G., Implicit-explicit schemes for BGK kinetic equations, J. Sci. Comp., 32(1), 1–28, 2007

[53] M. K. Gobbert T. S. Cale, A kinetic transport and reaction model and simulator for rarefied gas flow in the transition, J. Comp. Phys. , 213 (2), 591–612, 2006

[54] Alekseenko, A., Gimelshein, N., Gimelshein, S, An application of Discontinuous Galerkin space and velocity disretisations to the solution of a model kinetic equation, International Journal of Computational Fluid Mechanics, 26, (1-5), pp141–161, 2012

[55] Xu, K., Discontinuous Galerkin BGK method for viscous flow equations: one-dimensional systems. SIAM Journal on Scientific Computing, 25, pp 1941–1963, 2004

[56] Xiong, T. et al, High Order Asymptotic Preserving Nodal Discontinuous Galerkin IMEX Schemes for the BGK Equation, J. Comp. Phys.,284,70–94, 2015

[57] B. Evans K. Morgan O. Hassan, A discontinuous Taylor-Galerkin finite element approach for solution of the collisionless Boltzmann equation, Proceedings of the 14th ACME Conference: Queen's University, Belfast, 135–138, 2006

[58] J.N. Moss, G.A. Bird, Direct Simulation of Transitional Flow for Hypersonic Re-entry Conditions, *AIAA*

Paper no. 84-0223, 1984

[59] M.M. Kuzetsov, Analytical Solution of the Boltzmann Equation in a Knudsen Layer, *J.* App. Mech. & Tech. Phys., **4**(2), 604–607, 1971

[60] S.A. Trugman, A.J. Taylor, Analytic solution of the Boltzmann equation with applications to electron transport in inhomogeneous semiconductors, *P*hys. Rev. B , **33**(8), 5575–5584, 1986.

[61] W.G. Vincenti, Introduction to Physical Gas Dynamics, *John Wiley and Sons, Inc.*, New York, 1965

[62] P.L. Bhatnagar E.P. Gross M. Krook, Model for collision processes in gases, I Small amplitude processes in charged and neutral one-component systems, *Phys. Rev.*, **94**, 511–524, 1954.

[63] Cockburn, Shu, TVB Runge-Kutta local projection discontinuous Galerkin finite element method for conservation laws II: general framework, 52 (186), *Math. Comp.*,411–435, 1989

[64] J. Donea, A Taylor–Galerkin Method for Convective Transport, *Int. J. Numer. Meth. Fluids*, **20**, 101–120, 1984.

[65] N. Bellemo, P. LeTallec, B. Perthame, Nonlinear Boltzmann equation solutions and applications to fluid dynamics, *App. Mech. Rev.*, **48** (12), 1995.

[66] C. Cercignani, Theory and Application of the Boltzmann Equation, *Springer*, 1988.

[67] G. Busoni, A. Palczewski, A stationary Boltzmann equation near equilibrium, *Math Models Methods Appl. Sci.*, **3**, 395–440, (1993).

[68] J.C. Maxwell, *"On the dynamic theory of gases"*, Phil. Trans. Soc., 157, (49), 1867.

[69] G. Karypis, V. Kumar, METIS4.0: Unstructured graph partitioning and sparse and sparse matrix ordering system. Technical report, Department of Computer Science, University of Minnesota (1998), http://www.cs.unn.edu/ metis

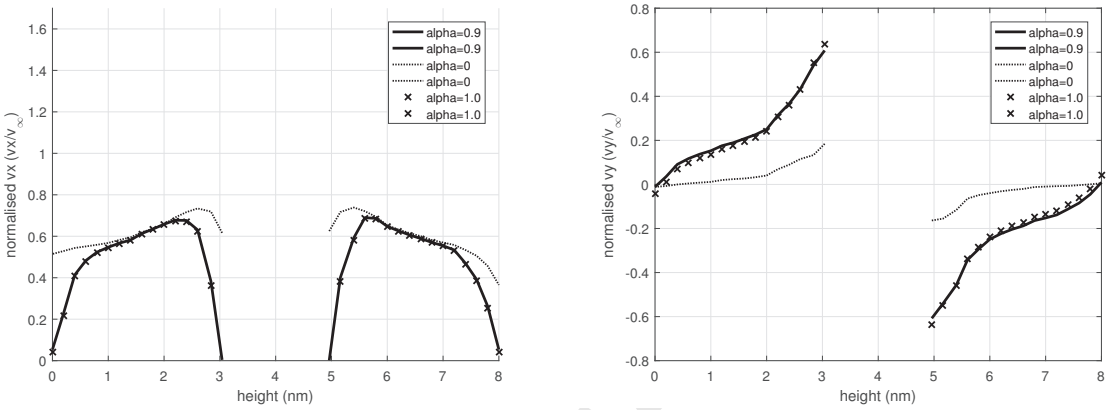

$(a) v_x/\left|\mathbf{v}\right|_\infty, 1234$

$(b) v_y/\left|\mathbf{v}\right|_\infty, 1234$

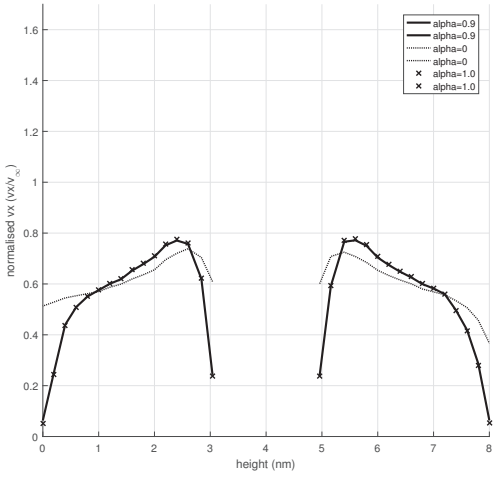

$(c) v_x/\left|\mathbf{v}\right|_\infty, 5678$

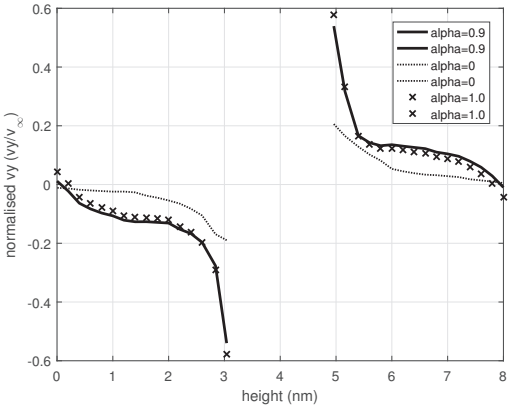

$(d) v_y/\left|\mathbf{v}\right|_\infty, 5678$

Figure 15: $Re_\infty = 1.0$ bulk velocity (v_x and v_y component) distributions at $\alpha = 0.0, 0.9, 1.0$ on lines 1234 ((a),(b)) and 5678 ((c),(d))

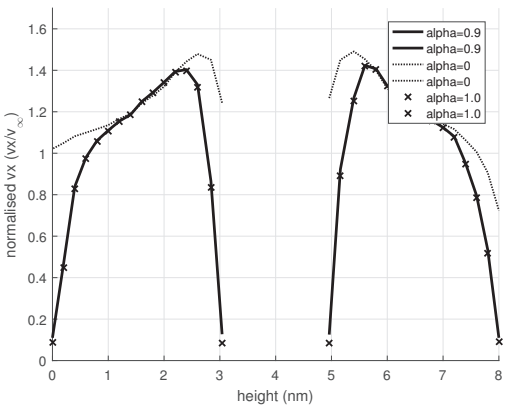

$(a) v_x/\left|\mathbf{v}\right|_\infty, 1234$

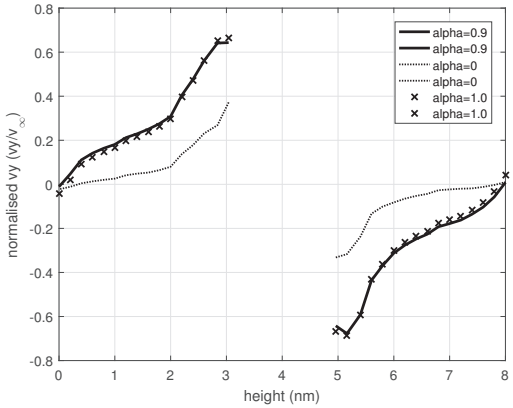

$(b) v_y/\left|\mathbf{v}\right|_\infty, 1234$

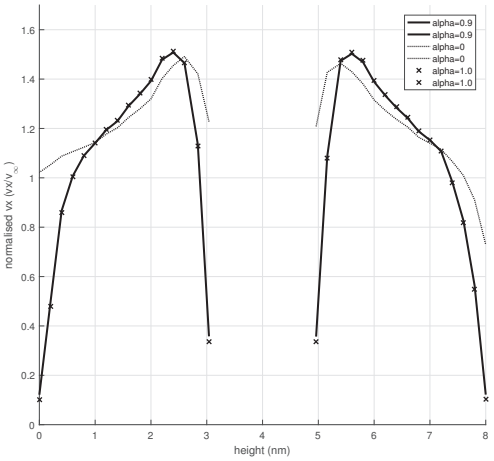

$(c) v_x/\left|\mathbf{v}\right|_\infty, 5678$

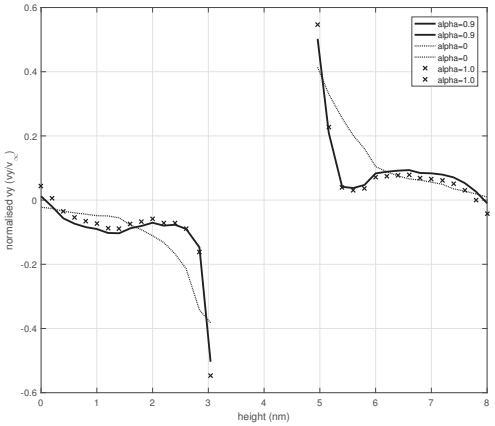

$(d) v_y/\left|\mathbf{v}\right|_\infty, 5678$

Figure 16: $Re_\infty = 2.0$ bulk velocity (v_x and v_y component) distributions at $\alpha = 0.0, 0.9, 1.0$ on lines 1234 ((a),(b)) and 5678 ((c),(d))

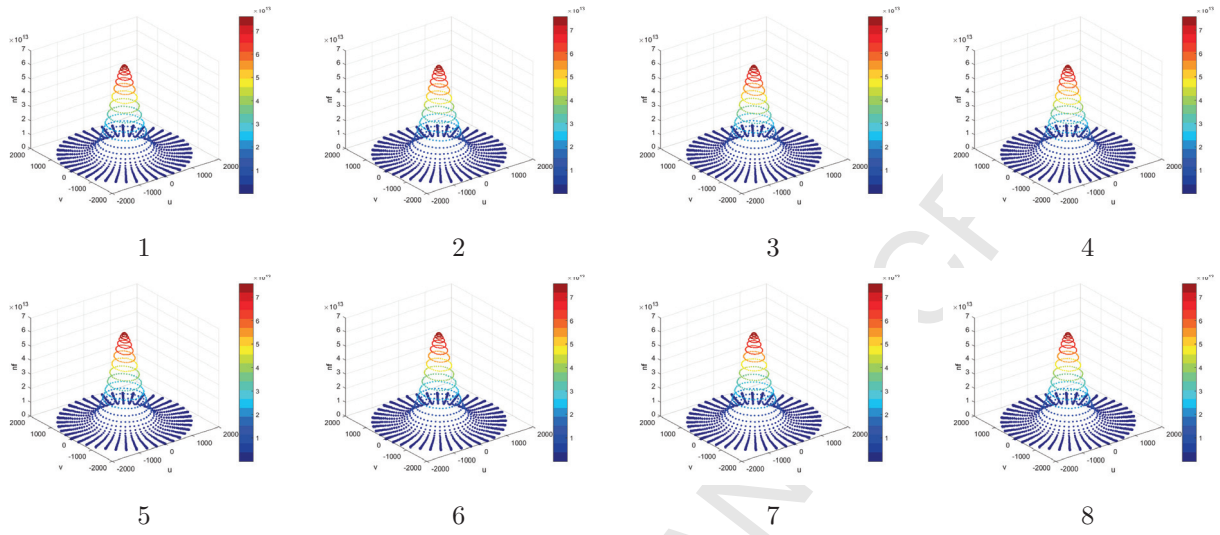

Figure 17: Re=2.0 α=0.9 molecular distribution functions ($nf = f(c_x, c_y)$) at points 1,2,3,4,5,6,7,8 with reference to Figure 13

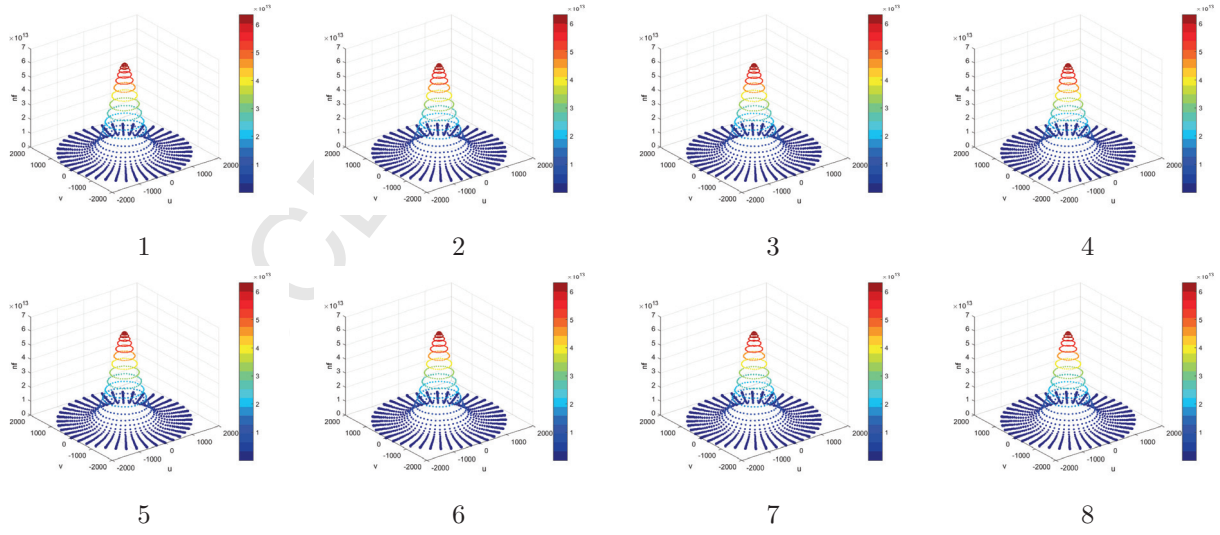

Figure 18: Re=0.25 α=0.9 molecular distribution functions ($nf = f(c_x, c_y)$) at points 1,2,3,4,5,6,7,8 with reference to Figure 13

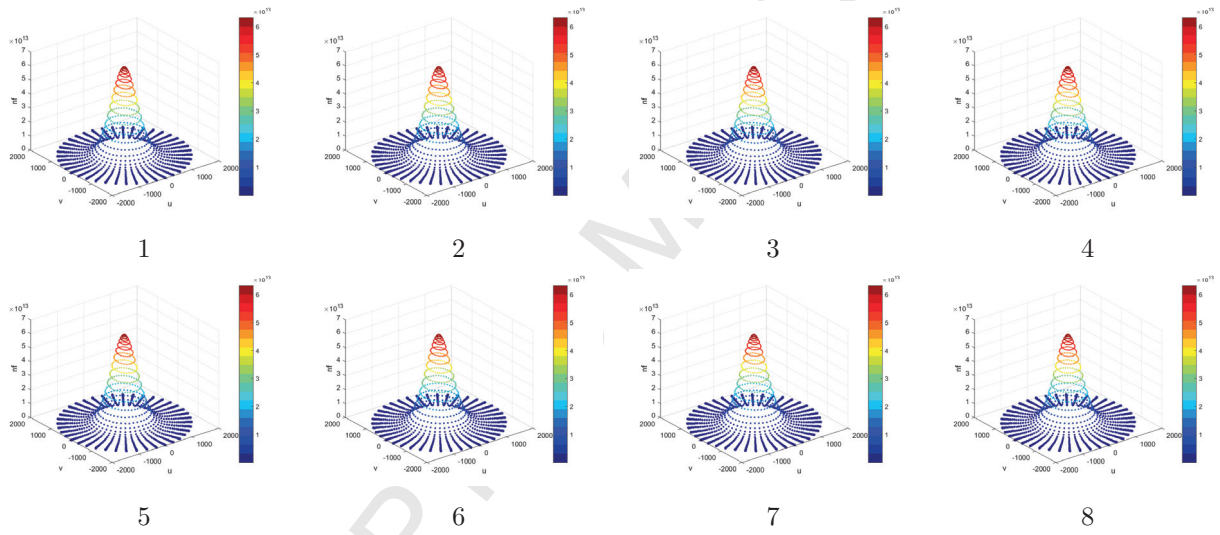

Figure 19: Re=2.0 α=0.0 molecular distribution functions ($nf = f(c_x, c_y)$) at points 1,2,3,4,5,6,7,8 with reference to Figure 13